RSC Advances

PAPER

View Article Online
View Journal | View Issue

Cite this: *RSC Adv.*, 2015, **5**, 90621

Carbon monoxide interactions with pure and doped $B_{11}XN_{12}$ (X = Mg, Ge, Ga) nano-clusters: a theoretical study

Alireza Soltani*[ab] and Masoud Bezi Javan[c]

Received 29th June 2015
Accepted 8th September 2015

DOI: 10.1039/c5ra12571e

www.rsc.org/advances

The goal of this investigation was to study a novel sensor for detecting the toxic gas compounds of CO using $B_{11}XN_{12}$ (X = Ge, Mg, and Ga) nano-clusters in terms of its energetic, geometric, and electronic structure using DFT calculations by the PBE-D method. The reaction of CO gas with these doping atoms results in a weak interaction and an elongation of X–N bond of $B_{11}XN_{12}$ nano-clusters. After the adsorption of CO gas over the doped positions of $B_{11}XN_{12}$ nano-cluster, the conductivity of the adsorbent and the atomic charges in some of the nearby B and N atoms around X atoms were dramatically enhanced. These calculations represent the capabilities of the $B_{11}XN_{12}$ nano-clusters in designing novel materials based on $B_{11}XN_{12}$ for potential applications in gas sensing.

1. Introduction

Carbon monoxide or CO is an extremely poisonous gas to human and animal bodies when encountered in concentrations above 35 ppm. It is a colourless, poisonous and odourless gas; these characteristics make it one of the most fatal gases with a significant role in air pollutants and in human daily life. Due to increasing concern over the safety and health hazards related to this gas, there is an increasing demand of CO sensors.[1–3] Thus, theoretical studies regarding the adsorption and dissociation of CO molecule using the Rh-decorated SWCNT,[4] Fe–$B_{18}N_{18}$ cluster,[5] Al–graphitic boron nitride sheet,[6] Al/Ga-doped BN nanotube,[7] FeCo alloy (110) surface,[8] ZnO (1010) surface,[9] $B_{12}N_{12}$ nano-cage,[10] doped h-BN monolayer,[11] and transition metal doped BN nanotube[12] have been reported. In particular, theoretical studies have shown that some metal-doped BN nanostructures are promising candidates to act as chemical sensors.[13–17] During the last decade, various types of BN-based nanostructures consisting of nanotubes, nanohorns, nanoparticles, nanosheets, and nano-cages, have attracted considerable attention due to their unique chemical and physical properties.[18–20] $B_{12}N_{12}$ is one of the known stable class of small III–V nano-clusters with the network of B–N bonds, which is energetically favorable. The 4-membered rings of $B_{12}N_{12}$ consist of the B–N bonds, which result in angular strain in the network. Since then, B_iN_i clusters have been widely investigated both theoretically and experimentally.[21–26] Recently, Oku *et al.*[27] synthesized $B_{12}N_{12}$, which can be detected by laser desorption time-of-flight mass spectrometry. Their study indicated that a BN nano-cluster is a structure built from four squares and six hexagons rings. In addition, Matxain and co-workers theoretically studied the electronic structure and the energy differences between covalent and van der Waals dimers using the hybrid B3LYP and MPW1PW91 density functional theory.[28] Li *et al.* proposed bonding character and electronic structure of $B_{12}C_6N_6$ fullerene using *ab initio* calculations.[29] They found that replacing an N atom with a C atom in the $B_{12}N_{12}$ nano-cage results in a decrease of the cluster energy gap. Bahrami and co-authors reported a theoretical study of amphetamine adsorption upon the pure P-doped and Al-doped $B_{12}N_{12}$ nano-cage at the M06-2X/6-311++G** level of theory.[30] Based on their results, the pure $B_{12}N_{12}$ nano-cage has a better condition for detecting amphetamine compared with the P-doped and Al-doped $B_{11}N_{12}$ nano-cage. Doping in BN nanomaterials can outstandingly alter the electronic properties, which can be utilized to develop its sensing applicability. Previous reports demonstrated the reaction of different molecules with the pure and doped metal BN nanostructures using DFT calculations.[31–33] In this study, we investigated the interaction of CO molecule with the pure Ga, Ge, and Mg atoms of $B_{11}XN_{12}$ nano-clusters to find whether these adsorbents can be used as a gas sensor in environmental monitoring using DFT calculations.

2. Computational details

To study the structural parameters and electronic properties of the pure $B_{11}XN_{12}$ (X = Ge, Mg, and Ga) nano-cluster and that interacted with a CO molecule, we carried out density functional theory (DFT) calculations. The goal is to calculate equilibrium geometries, adsorption energies, Mulliken population charge

[a]*Joints, Bones and Connective Tissue Research Center, Golestan University of Medical Science, Gorgan, Iran. E-mail: Alireza.soltani46@yahoo.com; Tel: +98-938-4544921*

[b]*Young Researchers and Elite Club, Gorgan Branch, Islamic Azad University, Gorgan, Iran*

[c]*Physics Department, Faculty of Sciences, Golestan University, Gorgan, Iran*

analysis (MPA), molecular electrostatic potential (MEP), frontier molecular orbital (FMO), and density of states (DOS) analyses for these complexes. All the geometry optimizations and energy calculations were performed using GAMESS software[34] at the level of density functional theory (DFT) using PBE functional augmented with an empirical dispersion term (PBE-D) and 6-311G** standard basis set. Moreover, the corresponding optical adsorption spectra were obtained through time-dependent density functional theory (TD-DFT) calculations in the gas phase regime.[35–37] The relaxed structures were further subjected to the computations for harmonic vibrational frequencies at the PBE functional. For all the systems, the SCF convergence limit was set to 10^{-6} a.u. over energy and electron density. The basis set superposition error (BSSE) for the adsorption energy was corrected by implementing the counterpoise method.[38,39] The adsorption energies (E_{ad}) for each of the structures were determined at 298.15 K and 1 atm using the following formulae:

$$E_{ad} = E_{B12N12\text{–}CO} - (E_{B12N12} + E_{CO}) + E_{BSSE} \quad (1)$$

$$E_{ad} = E_{B11XN12\text{–}CO} - (E_{B11XN12} + E_{CO}) + E_{BSSE} \quad (2)$$

where $E_{B11XN12\text{–}CO}$ is the total energy of the $B_{11}XN_{12}$ nanocage interacting with the CO molecule. $E_{nano\text{-}cage}$ and $E_{TM\text{-}nano\text{-}cage}$ are the total energies of the pure and $B_{11}XN_{12}$, respectively, and E_{CO} is the total energy of an isolated CO molecule. The electrophilicity index (ω) concept was stated for the first time by Parr *et al.*[40,41] Chemical potential (μ) is defined according to the following equation:

$$\mu = -\chi = -1/2(I + A) \quad (3)$$

Electronegativity (χ) is defined as the negative of chemical potential, as follows: $\chi = -\mu$. According to Koopmans theorem,[42] chemical hardness (η) can be approximated by the following equation:

$$\eta = 1/2(I - A) \quad (4)$$

$I(-E_{HOMO})$ is the ionization potential and $(-E_{LUMO})$ is the electron affinity of the molecule. E_{HOMO} is the energy of the highest occupied molecular orbital and E_{LUMO} is the energy of the lowest unoccupied molecular orbital of the considered structure. Softness (S) and electrophilicity index are determined by the following equations, respectively:

$$S = 1/2\eta \quad (5)$$

$$\omega = (\mu^2/2\eta) \quad (6)$$

3. Results and discussion

First, the $B_{12}N_{12}$ nano-cage was optimized as an adsorbent for detection of CO molecule at the gas phase using PBE-D method and 6-311G** standard basis set (see Fig. 1). Then, two stable states of the CO adsorption were considered, which locates the C and O over top of a B atom of $B_{12}N_{12}$ nano-cage. When CO molecule is adsorbed from C and O heads toward the boron atom of the adsorbent, the adsorption energies and distances of CO physisorption are −0.27 eV (II: 1.655 Å) and −0.06 eV (III: 3.176 Å) respectively (Table 1). Regarding previous studies, the adsorption of a CO molecule over (5, 5) SWCNT and capped CNT in their most stable states are about −0.147 and −0.02 eV.[1,43] Baierlea *et al.* and Beheshtian *et al.* showed that the BN nanotubes have physical interactions with CO molecule in the range of about −0.13 and −0.06 eV.[13,44] Our results were in agreement with the study of Beheshtian and co-workers, who reported a DFT study of CO molecule in reaction with $B_{12}N_{12}$ nano-cluster.[10] They showed that CO can be adsorbed over the nano-cluster with the adsorption energy of 0.15–0.30 eV. It was found that the length of C≡O bond (1.1386 Å at the PBE-D) after reaction with $B_{12}N_{12}$ is slightly smaller than that of a free CO molecule (1.357 Å), which is close to the reported experimental value of 1.128 Å.[45] By Mulliken charge analysis, a charge transfer of about 0.172*e* (C head) and 0.019*e* (O head) occurs from CO molecule (electron donor) to $B_{12}N_{12}$ nano-cluster. In Fig. 1, the density of states are shown for the different CO-adsorptions over the $B_{12}N_{12}$ nano-cluster discussed above. Compared with the DOS of the pristine nano-cluster, the adsorption of CO molecule alters the electronic structure of $B_{12}N_{12}$, as shown in Fig. 1. This indicates a remarkable change (II) of energy gap (E_g) of about 45.8%. The DOS plots of the complex clearly reveal that the LUMO level has a distinct change after the adsorption process.

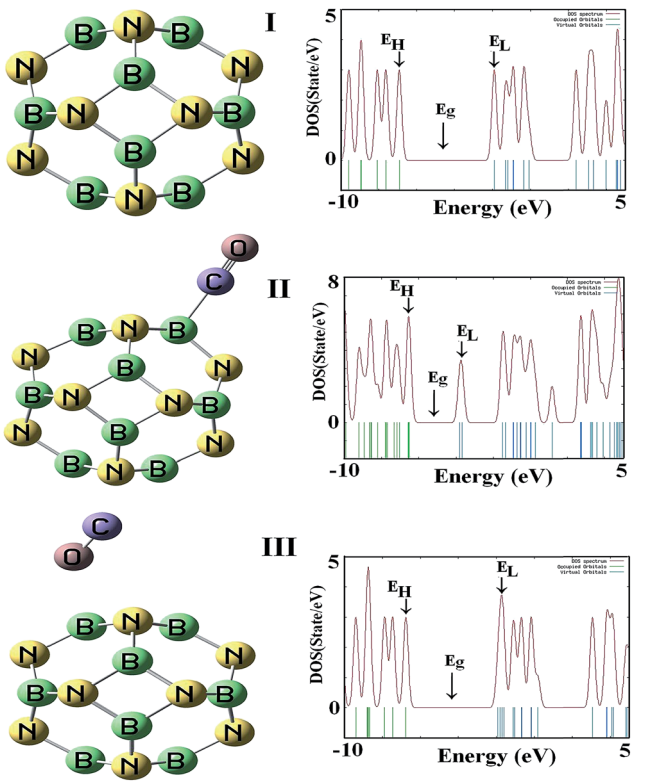

Fig. 1 Optimized structures and density of state spectra of CO and $B_{12}N_{12}$ nano-clusters.

Table 1 Calculated bond length, adsorbate-surface distance D/Å, adsorption energy E_{ad}/eV, HOMO energies (E_{HOMO}/eV), LUMO energies (E_{LUMO}/eV), dipole moment (DM/Debye), Fermi level energies (E_F/eV) and HOMO–LUMO energy gap (E_g/eV) for the pure $B_{12}N_{12}$ nano-cluster

System	E_{ad}/eV	D/Å	C–O/Å	B–N/Å	E_{HOMO}/eV	E_g/eV	E_{LUMO}/eV	ΔE_g%	E_F/eV	DM/Debye
CO	—	—	1.1386	—	−8.87	7.03	−1.84	—	−5.36	0.226
I	—	—	—	1.493	−6.91	5.0	−1.91	—	−4.41	0.00
II	−0.27	1.655	1.136	1.563	−6.52	2.71	−3.81	−45.8	−5.17	3.62
III	−0.06	3.176	1.139	1.495	−6.90	4.81	−2.09	−3.80	−4.50	0.182

In this stage, first, the optimized structures and density of states of the perfect $B_{12}N_{12}$ nano-cluster with doped transition metal atoms containing Mg, Ge, and Ga are used to calculate the adsorption of a CO molecule, as shown in Fig. 2. The length of Mg–N, Ge–N, and Ga–N bonds of the doped nano-cluster are calculated with values of 2.079, 1.946, and 1.921 Å, respectively. In a similar study, Li *et al.* generated a similar structure by replacing N with C atom in the $B_{12}N_{12}$ nano-cage using *ab initio* calculations.[29] Soltani *et al.*[7] determined the length of a Ga–N bond of a $B_{11}XN_{12}$ nano-cage to be about 2.072 Å. As reported in Table 2, the angles of the N–Mg–N, N–Ge–N, and N–Ga–N bonds of $B_{11}XN_{12}$ nano-cluster were found to be about 69.66°, 76.92°, and 79.76°, respectively. As shown in Fig. 2, all the doped systems with Mg, Ge, and Ga atoms in $B_{11}XN_{12}$ nano-cluster belong to C_s point group, while the point group symmetry of $B_{12}N_{12}$ nano-cage is T_h.[46] In the $B_{11}XN_{12}$ nano-cluster, metal atoms move slightly out of the cluster form leading to a significant change of the local geometry of the nano-cluster. The point charges over the Mg, Ge, and Ga atoms in $B_{11}XN_{12}$ nano-cluster are 0.621, 0.720, and 0.739e, while the corresponding

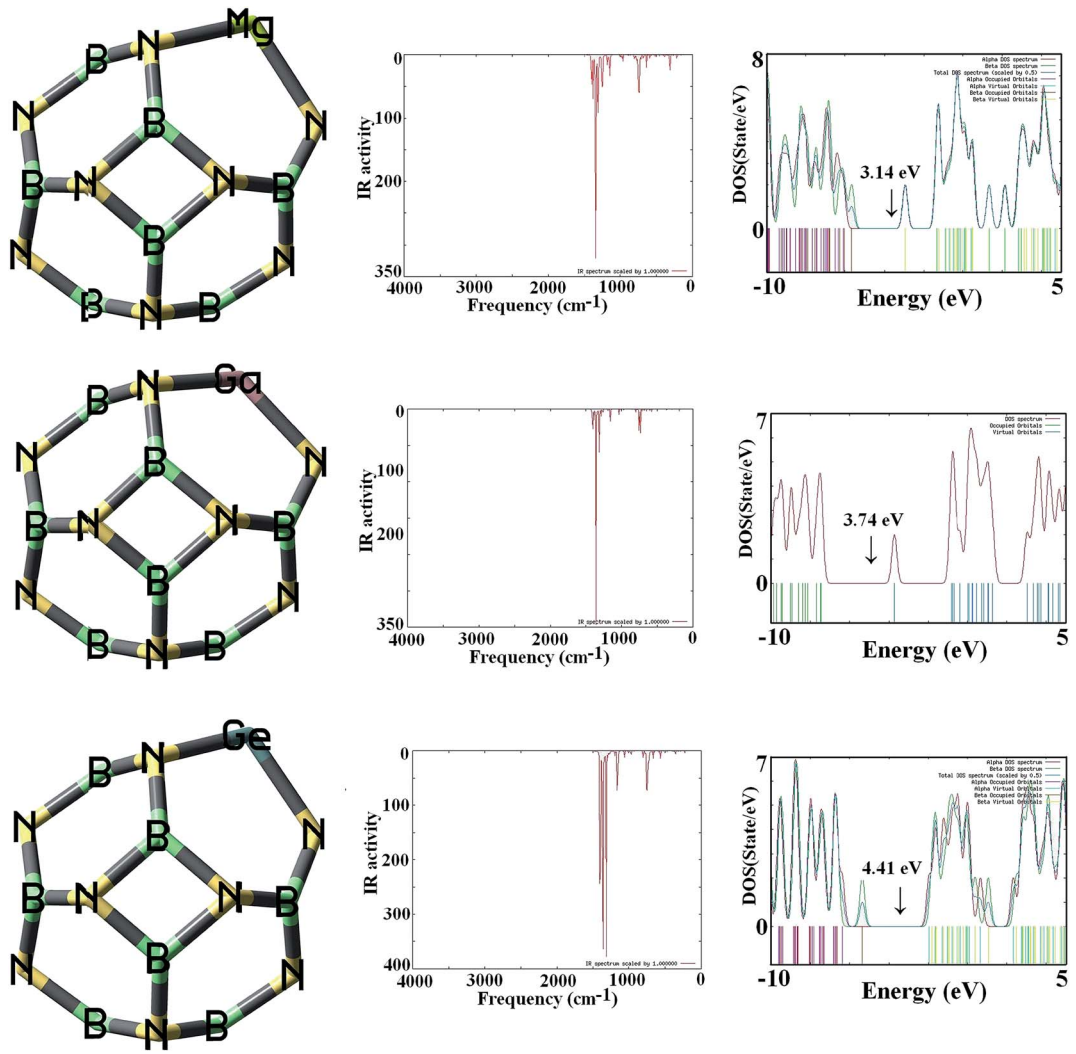

Fig. 2 Optimized structures, infrared and density of state spectra of $B_{11}XN_{12}$ nano-clusters.

Table 2 The obtained structural parameters for a single CO adsorption over the pure and $B_{11}XN_{12}$ nano-clusters

System	$R_{C=O}$	R_{Ga-N}	R_{Ge-N}	R_{Mg-N}	R_{N-Ga-N}	R_{N-Ge-N}	R_{N-Mg-N}
$GaB_{11}N_{12}$	—	1.921	—	—			
State I	1.144	1.923	—	—	117.889	—	—
State II	1.133	1.938	—	—	114.828	—	—
State III	1.132	1.937	—	—	114.707	—	—
State IV	1.137	1.910	—	—	120.488	—	—
$GeB_{11}N_{12}$	—		1.946				
State I	1.164	—	1.922	—	—	107.243	—
State II	1.140	—	1.947	—	—	105.975	—
State III	1.137	—	1.934	—	—	107.591	—
State IV	1.138	—	1.890	—	—	105.814	—
$MgB_{11}N_{12}$	—			2.079			
State I	1.132	—	—	2.098	—	—	105.671
State II	1.138	—	—	2.064	—	—	105.079
State III	1.146	—	—	2.088	—	—	110.126
State IV	1.203	—	—	2.010	—	—	106.710

values for N atoms are about −0.522, −0.512, and −0.503*e*, respectively. To better understand the properties of crucial transition states for the X-doped $B_{11}XN_{12}$ nano-cluster, we plotted frontier molecular orbitals (HOMO and LUMO) for these systems. These orbitals play an important role in governing many chemical reactions, and they are also responsible for charge transfer properties (see Fig. 3). By comparison, it is found that the HOMO and LUMO energy levels can be significantly changed due to doping atoms because the energy gap of the nanoclusters reduces in the process of CO adsorption. From HOMO and LUMO analysis, it is easily seen that there is a uniform shift of the HOMO level to the upper energy region due to the mutual charge transfer and the interaction between N atoms of the nano-cluster and dopant atoms.

The next stage involved search for a suitable nano-cluster for CO detection. After full optimization, adsorption states of CO molecule over the X-doped $B_{12}N_{12}$ nano-cluster using PBE

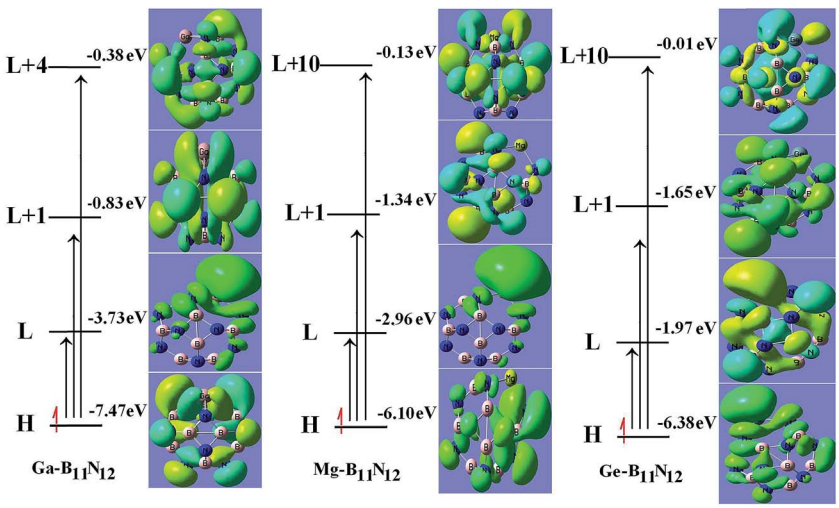

Fig. 3 Crucial transition states of $B_{11}XN_{12}$ structures with the largest component coefficient marked.

Table 3 Calculated bond length, adsorbate-surface distance *D*/Å, adsorption energy E_{ad}/eV, HOMO energies (E_{HOMO}/eV), LUMO energies (E_{LUMO}/eV), work function (Φ/eV), dipole moment (DM/Debye), Fermi level energies (E_F/eV) and HOMO–LUMO energy gap (E_g/eV) for X-doped $B_{11}N_{12}$ nano-cluster

System	E_{ad}/eV	*D*/Å	E_{HOMO}/eV	E_g/eV	E_{LUMO}/eV	ΔE_g%	E_F/eV	Φ/eV	DM/Debye
$GaB_{11}N_{12}$	—	—	−7.47	3.74	−3.73	—	−5.60	1.87	2.654
State I	−0.200	2.511	−6.36	2.83	−3.53	24.33	−4.95	1.42	6.492
State II	−0.657	2.148	−6.17	1.45	−4.72	61.23	−5.44	0.72	6.478
State III	−0.668	2.148	−6.19	1.45	−4.70	60.16	−5.44	0.74	2.556
State IV	−0.221	1.671	−6.28	5.023	−3.81	33.96	−5.04	1.23	4.562
$GeB_{11}N_{12}$	—	—	−6.38	4.41	−1.97	—	−4.18	2.21	1.673
State I	−0.132	2.179	−4.423	2.88	−1.54	−34.74	−2.98	1.44	1.577
State II	−0.067	3.476	−3.981	2.34	−1.64	−46.82	−2.81	1.17	1.188
State III	−0.163	1.685	−6.288	4.93	−1.36	11.68	−3.83	2.47	1.8203
State IV	−0.059	3.466	−6.270	4.73	−1.54	7.26	−3.91	2.37	1.840
$MgB_{11}N_{12}$	—	—	−6.10	3.14	−2.96	—	−4.53	1.57	5.249
State I	−0.589	2.270	−5.86	1.44	−4.42	54.14	−5.14	0.72	7.246
State II	−0.356	2.351	−5.90	4.741	−4.21	46.18	−5.0	0.79	5.38
State III	−0.871	1.681	−5.92	2.93	−2.99	6.69	−4.45	1.46	6.85
State IV	−0.073	1.358	−5.90	2.41	−3.49	23.25	−4.70	1.21	4.061

method were studied and are reported in Table 3. This method has shown to obtain reasonable results for dative B–N bonds in comparison with other methods.[47] In these interactions (Fig. 4–6), the CO molecule has electrostatic contact with the X-doped $B_{12}N_{12}$ nano-clusters. The observed trend for the $B_{11}GaN_{12}$ nano-cluster with CO molecule was found to be III > II > IV > I. In contrast, these values in the $B_{11}MgN_{12}$ were found to be III > I > II > IV, which means that the $B_{11}MgN_{12}$ is more stable than $B_{11}GaN_{12}$, whereas CO molecule is physisorbed toward $B_{11}GeN_{12}$ nano-cluster, which mainly stems from the van der Waals interaction, as can be seen in Table 3. According to the relative energy values, $B_{11}GeN_{12}$ is the least stable among all the species that interacted with the CO molecule. The minus value of adsorption energy in the interaction between adsorbent and adsorbate, representing that the CO molecule configuration has a very weak physical bond with the doping atoms of the nano-cluster. The weak type of interactions between adsorbate and adsorbent can be remarkable in gas detection because such ineffective interactions represent that the desorption of the adsorbate could be easy and the device can benefit from short recovery times.[48] If E_{ad} is significantly decreased, considerable shorter recovery time is expected. $\tau = \upsilon_0^{-1} e^{(-E_{ad}/k_B T)}$, where T is

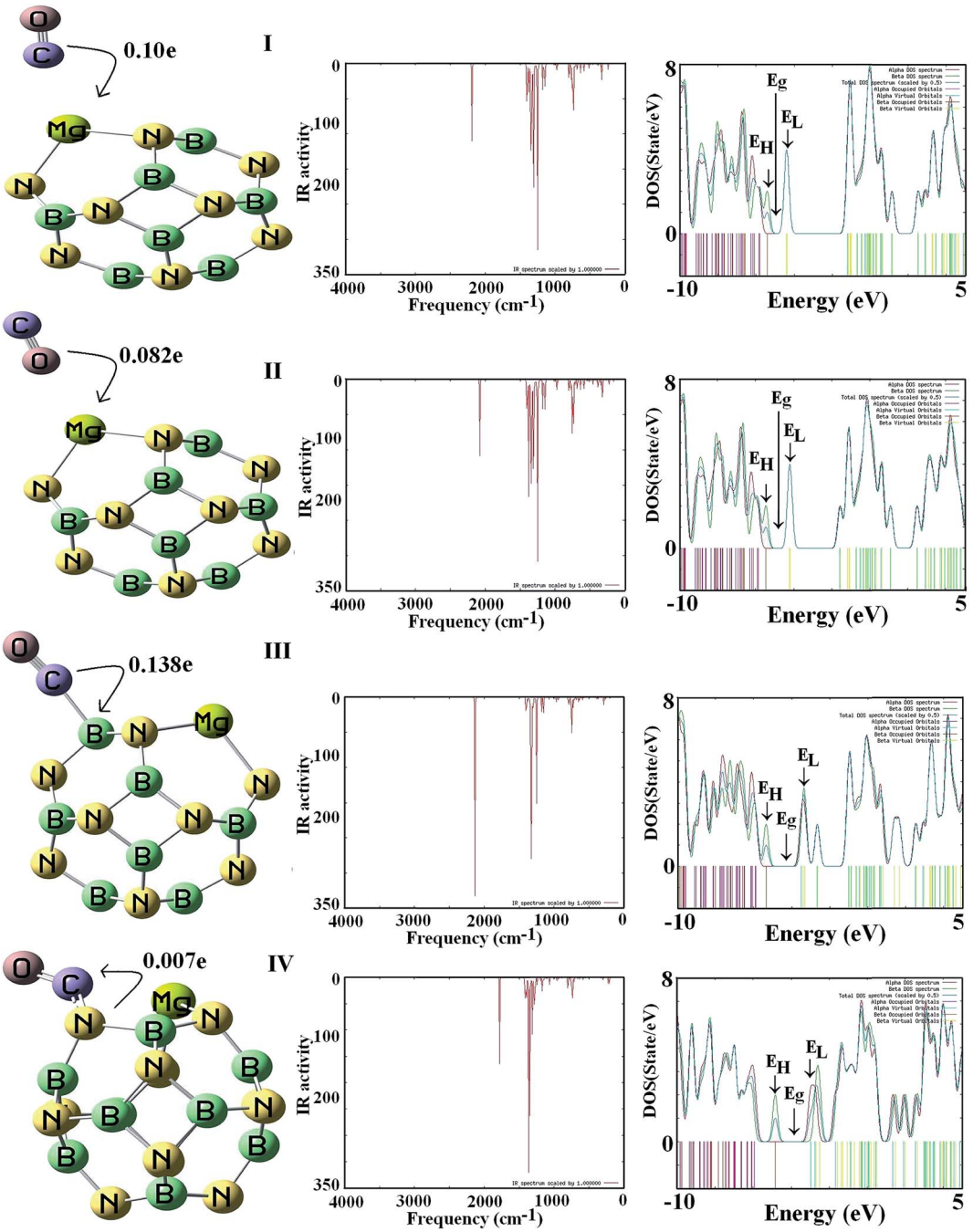

Fig. 4 Optimized structures, infrared and density of state spectra of $B_{11}MgN_{12}$ nano-clusters interacting with a CO molecule.

temperature, k_B is the Boltzmann constant (8.62×10^{-5} eV K^{-1}), and υ_0 is the attempt frequency. According to this equation, the $B_{11}XN_{12}$ nano-cluster should be a good CO sensor with quick response as well as short recovery time. Upon the interaction of the CO molecule with X-doped $B_{12}N_{12}$ nano-cluster, the Mg–N, Ga–N, and Ge–N bond lengths shift to 2.098, 1.938, and 1.890 Å, respectively, with a resulting change in hybridization from sp^2 to sp^3. As a result, the adsorption of CO over the $B_{11}GaN_{12}$ and $B_{11}MgN_{12}$ nano-clusters leads to the elongation of the bond length but in the $B_{11}GeN_{12}$, it shortens the bond-length (Table 2). Bahrami and co-workers studied the effects of Al-doped and P-doped $B_{12}N_{12}$ nano-cage at the M06-2X method.[30] They showed that the distance between the Al and the N atoms is about 1.97 Å. In addition, they reported that the adsorption of amphetamine on the surfaces of the perfect Al-doped and P-doped $B_{12}N_{12}$ nano-cages are found at −1.63, −2.48, and −0.33 eV, respectively. The results of these reports revealed that the Al-doped $B_{11}N_{12}$ can be used as an adsorbent in the environmental system.

To better understand the nature of CO adsorption over the electronic properties of adsorbent, we have carried out the electronic density of states (DOSs) analysis. The GaussSum program was used to obtain DOS results.[49] The DOS spectrum of these structures represent the HOMO–LUMO gaps of the X-doped BN

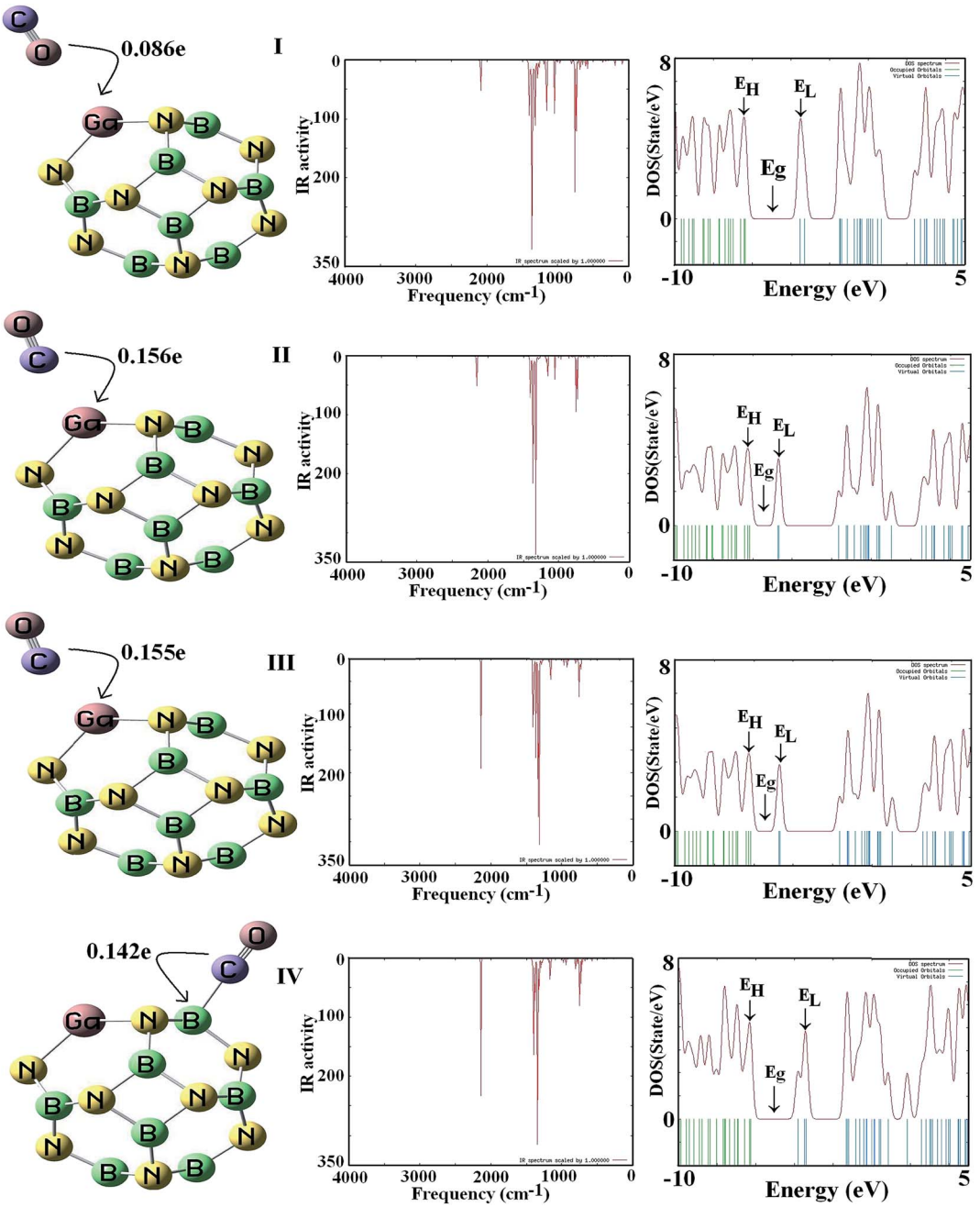

Fig. 5 Optimized structures, infrared and density of state spectra of $B_{11}GaN_{12}$ nano-clusters interacting with a CO molecule.

nano-clusters. E_g of Mg-doped, Ga-doped, and Ge-doped $B_{12}N_{12}$ nano-clusters are 3.14, 3.74, and 4.41 eV, while this value in the pure nano-cluster is about 5.0 eV. However, there is noticeable change in resistivity when the E_g for structures is decreased when compared to that of $B_{12}N_{12}$ nano-cluster. Oku and co-workers experimentally determined that the energy gap of the pure $B_{12}N_{12}$ nano-cluster is about 5.1 eV between HOMO and LUMO.[27] Thus, the accuracy of the theoretical calculation is close to the experimental data as mentioned above. In the most stable configurations, after the CO adsorption toward the Mg, Ga, and Ge atoms of $B_{11}XN_{12}$ nano-clusters, ΔE_g of these configurations significantly changed by about 54.14%, 61.23%, and 46.82%, respectively. This result implies that the electronic properties of the $B_{11}GaN_{12}$ nano-cluster are very sensitive to the CO adsorption in comparison with the pure $B_{12}N_{12}$ nano-cluster. Zhang *et al.* have shown that the graphitic BN sheet that by replacing Al-dopant and defects have high sensitive to the CO gas compared to the pure model.[6] Moreover, their results indicated that the vacancy-defect g-BN has more change of energy gap than Al-dopant g-BN. As seen in Table 3, DOS spectrum in the CO/$B_{11}GaN_{12}$ complex (State II) near both of the valence and conduction levels have distinct changes in comparison with that

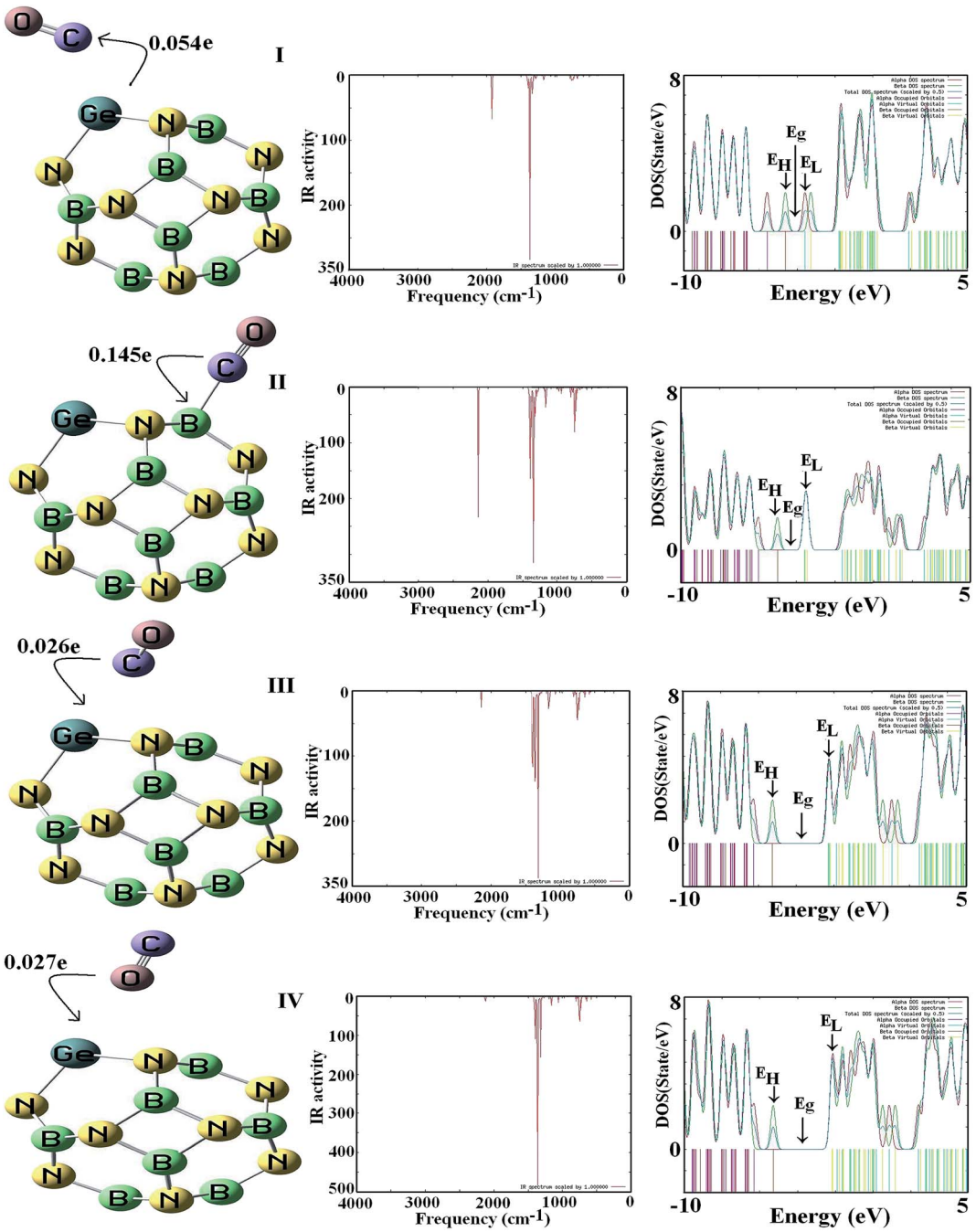

Fig. 6 Optimized structures, infrared and density of state spectra of $B_{11}GeN_{12}$ nano-clusters interacting with a CO molecule.

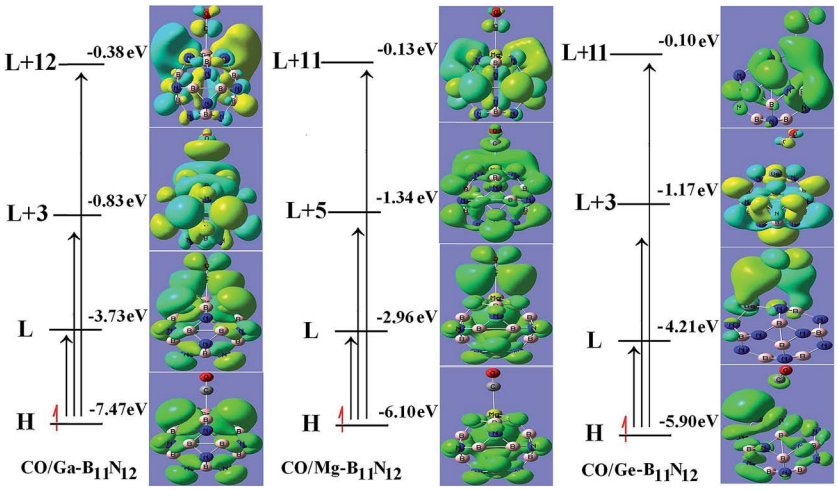

Fig. 7 Crucial transition states of the $B_{11}XN_{12}$ structures interacting with CO with the largest component coefficient marked.

in the $B_{12}N_{12}$. The valence level (−3.981 eV) of the $CO/B_{11}GeN_{12}$ complex (State II) exhibits a distinct change when compared to that of $B_{12}N_{12}$ (−6.38 eV). DOS spectrum for the $CO/B_{11}GeN_{12}$ complex (State I) revealed that the conduction level (−4.42 eV) of this complex exhibits a distinct change in comparison with that of $B_{12}N_{12}$ (−2.96 eV). This reports leads to a slight reduction in the work function that is important in the field emission applications. The values of Φ for the adsorption of CO gas, in the most stable models (Table 3), upon the Mg, Ga, and Ge atoms of $B_{11}XN_{12}$ nano-cluster are considerably decreased from 1.57, 1.87, and 2.21 eV to 0.72 (State I), 0.72 (State II), and 1.17 eV (State II), respectively. The decrement in the work function (Φ) values reveals that the field emission properties of the nano-clusters are more noticeable on the adsorption of CO gas because the electrons can be pulled from the surface more easily.[50,51] In Fig. 7, the crucial excited states for the interaction of CO molecule with $B_{11}XN_{12}$ nano-cluster are provided, where the electron cloud in their LUMO, LUMO+3, and LUMO+5 are dominant over the CO molecule, while electron cloud in their HOMO orbitals do not have the same distribution of the electron density. To explore the interaction mechanism between CO and the $B_{11}XN_{12}$ nano-cluster, we studied molecular electrostatic potential (MEP) maps for these processes, where the positive charges over the X-doped $B_{12}N_{12}$ nano-cluster are represented by the blue colors (see Fig. 8). MEP plots are computed at an isovalue of 0.0004 e au^{-3}. As demonstrated in these configurations, the CO molecule with blue color (positive charge) acts as an electron donor in the adsorption process. Most negative and natural regions of the MEP plots are colored yellow and green, respectively. Table 4 implies to the values of the quantum molecular descriptors computed for the adsorption of CO gas toward the $B_{11}XN_{12}$ nano-cluster. When CO gas reacts with the Mg-, Ga-, and Ge-doped $B_{12}N_{12}$ nano-cluster, the global hardness in the position of Ga and Mg dopants have the highest amount of hardness, while the lowest amount is in relation with the Ge dopant. In addition, when CO gas interacts with the $B_{11}XN_{12}$ nano-cluster, the η values have significant gain from 1.87, 1.57 and 2.21 eV in the Ga-, Mg-, and Ge-doped $B_{12}N_{12}$ nano-cluster to 2.54 eV (III), 2.59 eV (V), and 2.56 eV (V) after the adsorption of CO, respectively (see Table 4). For the suitable species, $B_{11}GaN_{12}$/CO, the global hardness of the complex is significantly increased and the electrophilicity of the complex is significantly reduced, indicating that the reactivity of the complex is decreased and also indicating that the stability of the complex is increased.[52] The electrophilicity index of the Ga-, Mg- and Ge-doped $B_{12}N_{12}$ nano-clusters were higher than that of the CO molecule, suggesting a charge transfer from adsorbate to adsorbent.[53–55]

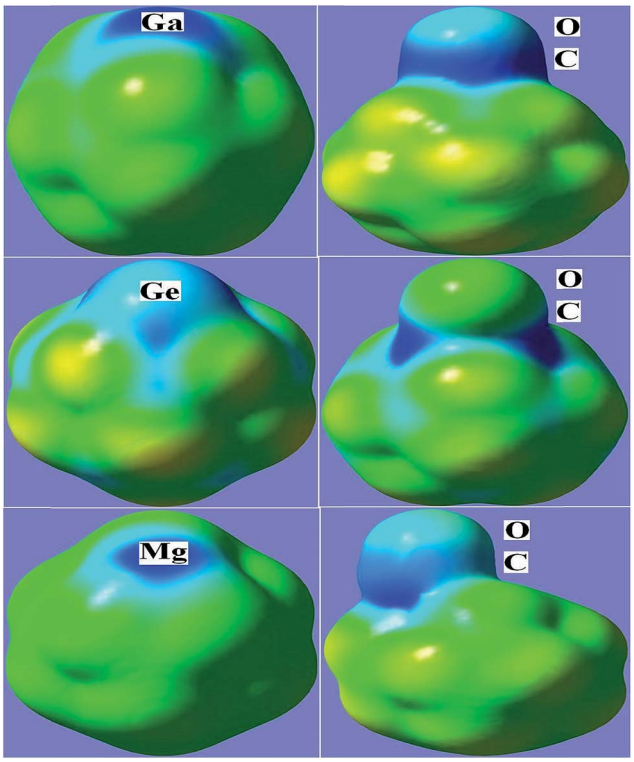

Fig. 8 Calculated electrostatic potentials with a density isosurface of 0.0004 electrons au^{-3}. The scale bar is in atomic units.

Table 4 Calculated quantum molecular descriptors for the CO molecule interacting with the $B_{11}XN_{12}$ nano-cluster

System	I/eV	A/eV	η/eV	μ/eV	ω/eV	χ/eV	S/eV
$GaB_{11}N_{12}$	7.47	3.73	1.87	−5.6	8.38	5.6	0.27
State I	6.16	1.244	2.46	−3.70	2.79	3.70	0.20
State II	6.38	1.383	2.49	−3.88	3.02	3.88	0.20
State III	6.57	1.483	2.54	−4.03	3.18	4.03	0.196
State IV	6.310	1.287	2.51	−3.80	2.87	3.80	0.199
State V	6.482	1.197	2.64	−3.84	2.79	3.84	0.189
$GeB_{11}N_{12}$	6.38	1.97	2.21	−4.18	3.95	4.18	0.226
State I	4.423	1.545	1.44	−2.98	3.09	2.98	0.347
State II	3.981	1.636	1.17	−2.81	3.63	2.81	0.426
State III	6.288	1.363	2.46	−3.83	2.97	3.83	0.203
State IV	6.270	1.540	2.37	−3.91	3.22	3.91	0.211
State V	6.328	1.212	2.56	−3.77	2.78	3.77	0.195
$MgB_{11}N_{12}$	6.10	2.96	1.57	−4.53	6.53	4.53	0.318
State I	5.901	1.086	2.41	−3.49	2.53	3.49	0.207
State II	5.948	1.207	2.37	−3.58	2.70	3.58	0.210
State III	5.958	0.990	2.48	−3.47	2.43	3.47	0.201
State IV	6.178	1.318	2.43	−3.75	2.89	3.75	0.205
State V	6.077	0.903	2.59	−3.49	2.35	3.49	0.193

In addition, to investigate the stability of X-doped $B_{12}N_{12}$ nano-clusters, the calculation of the harmonic frequencies for all the adsorption models is needed. The vibrational frequencies of the Mg–N, Ga–N, and Ge–N in $B_{11}XN_{12}$ nano-clusters are at 590, 610 and 562 cm^{-1}, respectively. IR vibrational spectrum indicates two active vibration modes (B–N bond) of $B_{12}N_{12}$ at 755 and 1375 cm^{-1} by the PBE-D method, which are in good agreement with the corresponding theoretical values of 1294 and 825 cm^{-1} by Pokropivny *et al.*[56] and 1649 and 909 cm^{-1} by Jensen and Toftlund.[57] Calculations over CO/$B_{11}MgN_{12}$ complex shows that the bond at 2190 cm^{-1} can be assigned to C–O molecule, while the values appearing at 1922 and 2159 cm^{-1} corresponds to the C–O stretching mode (from C head) of the CO adsorbed over $B_{11}GeN_{12}$ and $B_{11}GaN_{12}$ nano-clusters, respectively.

Herein, we use a TD-PBE/6-311G** calculation to study the optical properties of a CO molecule interacting with the $B_{11}XN_{12}$ nano-cluster.[58] In Table 5, we have presented the lowest excitation modes of the four most stable configurations of the adsorbing CO systems. For pure $B_{11}GaN_{12}$ systems, we have two considerable peaks at the energies of 2.44 and 2.66 eV because they are related to the H−1− > L and H−2− > L vertical transitions. In this case, the H → L transition has very low intensity, which shows the wave functions of the HOMO and excitation modes to the adsorption state. As for I and IV states, the first excitation energy interval is between 2.54–2.85 eV, while for II and III states, the lowest excitation energy range is about 1.5 eV. In all the considered CO adsorbed states, the contribution of the

Table 5 Selected excitation energies (eV, nm), oscillator strength (f), and relative orbital contributions calculated with the PBE method

Methods	Energy/eV	Wavelength/nm	Oscillator strength (f)	Assignment
Ga doping	2.44	508	0.0040	H−1 → L[a] (100%)
	2.66	465	0.0070	H−2 → L (100%)
State I	2.85	435	0.0016	H → L+1 (100%)
	2.90	428	0.0002	H−1 → L (100%)
State II	1.52	817	0.0084	H → L (99%)
	1.54	804	0.0003	H−1 → L (99%)
State III	1.51	818	0.0035	H → L (96%)
	1.53	806	0.0003	H−1 → L (99%)
State IV	2.54	488	0.0004	H−1 → L (100%)
	2.82	439	0.0105	H−2 → L (99%)
Mg doping	0.66	1891	0.0010	H → L (100%)
	1.17	1061	0.0006	H−1 → L (99%)
State I	0.71	1740	0.0011	H → L (100%)
	1.22	1013	0.0008	H−1 → L (99%)
State II	0.70	1780	0.0012	H−1 → L (99%)
	1.21	1024	0.0008	H−2 → L (64%)
State III	0.75	1646	0.0005	H−1 → L (99%)
	1.12	1101	0.0007	H−2 → L (98%)
State IV	1.47	840	0.0016	H−1 → L (100%)
	1.76	703	0.0020	H−2 → L (100%)
Ge doping	1.352	917	0.0020	H−1 → L (100%)
	1.433	865	0.0014	H−2 → L (100%)
State I	1.973	628	0.0001	H → L (98%)
	2.09	593	0.0032	H−1 → L (100%)
State II	1.46	848	0.0006	H−1 → L (100%)
	1.61	772	0.0021	H−2 → L (100%)
State III	1.41	878	0.0020	H−1 → L (100%)
	1.48	835	0.0011	H−2 → L (100%)
State IV	1.40	887	0.0020	H−1 → L (100%)
	1.47	842	0.0012	H−2 → L (100%)

[a] H and L are the highest occupied (HOMO) and lowest unoccupied molecular orbitals (LUMO), respectively.

H → L excitation has a noticeable growth. Similar trends also can be seen in corresponding Mg- and Ge-doped systems. Although the lowest excitation modes have a red shift in comparison with Ga-doped BN nanocage, in these cases, HOMO and LUMO have similar radial distribution on the cluster, which consequently results in low dipole moment and oscillation strength.

4. Summary

We have carried out density functional theory calculations over the adsorption of CO gas upon the Mg-, Ge-, and Ga-doped $B_{12}N_{12}$ nano-cluster. It was found that CO gas is weakly adsorbed over the $B_{11}XN_{12}$ nano-cluster due to van der Waals interaction between CO and the adsorbent. In addition, a slight reduction of the charge transfers in the adsorption process from CO to $B_{11}XN_{12}$ nano-cluster in comparison with the pure nano-cluster was observed. From the calculated results, we conclude that the electronic structure of the $B_{11}GaN_{12}$ undergoes a dramatic change after the CO adsorption process in comparison with the $B_{11}MgN_{12}$ and $B_{11}GeN_{12}$ nano-clusters. The $B_{11}GaN_{12}$ nano-cluster can act as a suitable sensor in the detection of CO gas by significantly changing the energy gap and work function of an adsorbent.

Acknowledgements

We thank the Sayad Shirazi Hospital, Golestan University of Medical Sciences, Gorgan, Iran. We also thank the Jaber Ebne Hayyan Unique Industry researchers Company, Gorgan city, Iran.

References

1 K. Liao, V. Fiorin, D. S. D. Gunn, S. J. Jenkinsa and D. A. King, *Phys. Chem. Chem. Phys.*, 2013, **15**, 4059.
2 S. Lin, X. Ye and J. Huang, *Phys. Chem. Chem. Phys.*, 2015, **17**(2), 888.
3 C. Yeh and J. Ho, *Phys. Chem. Chem. Phys.*, 2015, **17**, 7555.
4 J.-X. Zhao and Y.-H. Ding, *Mater. Chem. Phys.*, 2008, **110**, 411.
5 S. Nigam and C. Majumder, *ACS Nano*, 2008, **2**, 1422.
6 Y.-H. Zhang, K.-G. Zhou, X.-C. Gou, K.-F. Xie, H.-L. Zhang and Y. Peng, *Chem. Phys. Lett.*, 2010, **484**, 266.
7 A. Ahmadi Peyghan, A. Soltani, A. Allah Pahlevani, Y. Kanani and S. Khajeh, *Appl. Surf. Sci.*, 2013, **270**, 25.
8 P. Rochana and J. Wilcox, *Surf. Sci.*, 2011, **605**, 681.
9 Q. Yuan, Y.-P. Zhao, L. Li and T. Wang, *J. Phys. Chem. C*, 2009, **113**, 6107.
10 J. Beheshtian, Z. Bagheri, M. Kamfiroozi and A. Ahmadi, *Microelectron. J.*, 2011, **42**, 1400.
11 S. Sinthika, E. Mathan Kumar and R. Thapa, *J. Mater. Chem. A*, 2014, **2**, 12812.
12 M. Bezi Javan, *Surf. Sci.*, 2015, **635**, 128.
13 R. J. Baierlea, T. M. Schmidt and A. Fazzio, *Solid State Commun.*, 2007, **142**, 49.
14 Z. Liu, Q. Xue, T. Zhang, Y. Tao, C. Ling and M. Shan, *J. Phys. Chem. C*, 2013, **117**, 9332.
15 Q. Dong, X. M. Li, W. Q. Tian, X.-R. Huang and C.-C. Sun, *J. Mol. Struct.*, 2010, **948**, 83.
16 B. Gao, J.-X. Zhao, Q.-H. Cai, X.-G. Wang and X.-Z. Wang, *J. Phys. Chem. A*, 2011, **115**, 9969.
17 S. Lin, X. Ye, R. S. Johnson and H. Guo, *J. Phys. Chem. C*, 2013, **117**(33), 17319.
18 A. Nishiwaki, T. Oku and I. Narita, *Sci. Tech. Adv. Mater.*, 2004, **5**, 629.
19 T. Oku, K. Hiraga and T. Matsuda, *Mater. Trans.*, 2008, **49**, 2461.
20 C. Huang, W. Ye, Q. Liu and X. Qiu, *ACS Appl. Mater. Interfaces*, 2014, **6**(16), 14469.
21 V. V. Pokropivny, V. V. Skorokhod, G. S. Oleinik, A. V. Kurdyumov, T. S. Bartnitskaya, A. V. Pokropivny, A. G. Sisonyuk and D. M. Sheichenko, *J. Solid State Chem.*, 2000, **154**, 214.
22 J. Guo-Qiang, C. Xin and H. Zheng, *Chin. Phys. Lett.*, 2009, **26**, 033601.
23 A. V. Pokropivny, *Diamond Relat. Mater.*, 2006, **15**, 1492.
24 A. Soltani, M. T. Baei, M. Ramezani Taghartapeh, E. Tazikeh Lemeski and S. Shojaee, *Struct. Chem.*, 2015, **26**, 685.
25 A. Ahmadi Peyghan and H. Soleymanabadi, *Curr. Sci.*, 2015, **108**, 1910.
26 S. Yourdkhani, T. Korona and N. L. Hadipour, *J. Phys. Chem. A*, 2015, **119**, 6446.
27 T. Oku, A. Nishiwaki and I. Narita, *Sci. Tech. Adv. Mater.*, 2004, **5**, 635.
28 J. M. Matxain, L. A. Eriksson, J. M. Mercero, X. Lopez, M. Piris, J. M. Ugalde, J. Poater, E. Matito and M. Sola, *J. Phys. Chem. C*, 2007, **111**, 13354.
29 F. Li, Y. Zhang and H. Chen, *Phys. E*, 2014, **56**, 216.
30 A. Bahrami, S. Seidi, T. Baheri and M. Aghamohammadi, *Superlattices Microstruct.*, 2013, **64**, 265.
31 N. Injan, J. Sirijaraensreb and J. Limtrakul, *Phys. Chem. Chem. Phys.*, 2014, **16**, 23182.
32 N. L. Hadipour, A. Ahmadi Peyghan and H. Soleymanabadi, *J. Phys. Chem. C*, 2015, **119**(11), 6398.
33 A. Soltani, M. T. Baei, M. Mirarab, M. Sheikhi and E. Tazikeh Lemeski, *J. Phys. Chem. Solids*, 2014, **75**, 1099.
34 M. W. Schmidt, K. K. Baldridge, J. A. Boatz, S. T. Elbert, M. S. Gordon, J. H. Jensen, S. Koseki and N. Matsunaga, *et al.*, *J. Comput. Chem.*, 1993, **11**, 1347.
35 J. P. Perdew, K. Burke and M. Ernzerhof, *Phys. Rev. Lett.*, 1996, **77**, 3865.
36 S.-l. Tang, Y.-j. Liu, H.-x. Wang, J.-x. Zhao, Q.-h. Cai and X.-z. Wang, *Diamond Relat. Mater.*, 2014, **44**, 54.
37 Q. Sun, Z. Li, D. J. Searles, Y. Chen, G. Lu and A. Du, *J. Am. Chem. Soc.*, 2013, **135**, 8246.
38 F. Tournus and J.-C. Charlier, *Phys. Rev. B: Condens. Matter Mater. Phys.*, 2005, **71**, 165421.
39 M. T. Baei, M. Ramezani Taghartapeh, E. Tazikeh Lemeski and A. Soltani, *Superlattices Microstruct.*, 2014, **72**, 370.
40 R. G. Parr, R. A. Donelly, M. Levy and W. E. Palke, *J. Chem. Phys.*, 1978, **68**, 3801.
41 R. G. Parr, L. Szentpaly and S. Liu, *J. Am. Chem. Soc.*, 1999, **121**, 1922.
42 T. Koopmans, *Physica*, 1933, **1**, 104.

43 Z. Li and C.-Y. Wang, *Chem. Phys.*, 2006, **330**, 417.
44 J. Beheshtian, M. T. Baei and A. Ahmadi Peyghan, *Surf. Sci.*, 2012, **606**, 981.
45 D. R. Lide, *Handbook of Chemistry and Physics*, CRC, Florida, 1992.
46 H. Y. Wu, X. F. Fan, J.-L. Kuo and W.-Q. Deng, *Chem. Commun.*, 2010, **46**, 883.
47 M. T. Baei, *Comput. Theor. Chem.*, 2013, **1024**, 28.
48 J. Beheshtian, A. Ahmadi Peyghan and M. Noei, *Sens. Actuators, B*, 2013, **181**, 829.
49 N. M. O'Boyle, A. L. Tenderholt and K. M. Langner, *J. Comput. Chem.*, 2008, **29**, 839.
50 A. Ahmadi Peyghana, S. F. Rastegar and N. L. Hadipour, *Phys. Lett. A*, 2014, **378**, 2184.
51 J. Beheshtian, A. Ahmadi Peyghan and Z. Bagheri, *Sens. Actuators, B*, 2012, **171–172**, 846.
52 Z. Bolboli Nojini and S. Samiee, *J. Phys. Chem. C*, 2011, **115**, 12054.
53 P. K. Chattaraj, U. Sarkar and D. R. Roy, *Chem. Rev.*, 2006, **106**, 2065.
54 R. G. Parr, L. V. Szentpály and S. Liu, *J. Am. Chem. Soc.*, 1999, **121**, 1922.
55 S. Armaković, S. J. Armaković, J. P. Šetrajčić, S. K. Jaćimovski and V. Holodkov, *J. Mol. Model.*, 2014, **20**, 2170.
56 V. V. Pokropivny, V. V. Skorokhod, G. S. Oleinik, A. V. Kurdyumov, T. S. Bartnitskaya, A. V. Pokropivny, A. G. Sisonyuk and D. M. Sheichenko, *J. Solid State Chem.*, 2000, **154**, 214.
57 F. Jensen and H. Toftlund, *Chem. Phys. Lett.*, 1993, **201**, 89.
58 H. Ullah, A.-U.-H. Ali Shah, S. Bilal and K. Ayub, *J. Phys. Chem. C*, 2013, **117**, 23701.